University Library

MINERVA ACCESS

A gateway to Melbourne's research publications

Minerva Access is the Institutional Repository of The University of Melbourne

Author/s:
Masoomi-Godarzi, S;Liu, M;Tachibana, Y;Mitchell, VD;Goerigk, L;Ghiggino, KP;Smith, TA;Jones, DJ

Title:
Liquid Crystallinity as a Self-Assembly Motif for High-Efficiency, Solution-Processed, Solid-State Singlet Fission Materials

Date:
2019-08-01

Citation:
Masoomi-Godarzi, S., Liu, M., Tachibana, Y., Mitchell, V. D., Goerigk, L., Ghiggino, K. P., Smith, T. A. & Jones, D. J. (2019). Liquid Crystallinity as a Self-Assembly Motif for High-Efficiency, Solution-Processed, Solid-State Singlet Fission Materials. Advanced Energy Materials, 9 (31), https://doi.org/10.1002/aenm.201901069.

Persistent Link:
https://hdl.handle.net/11343/286092

Check for updates

Liquid crystallinity as a self-assembly motif for high efficiency, solution processed, solid-state singlet fission materials

*Saghar Masoomi-Godarzi, Maning Liu, Yasuhiro Tachibana, Valerie D. Mitchell, Lars Goerigk, Kenneth P. Ghiggino, Trevor A. Smith and David J. Jones**

Dedicated to Prof. Andrew Holmes on the occasion of his 75th birthday.

S. Masoomi-Godarzi, Dr. V. D. Mitchell, Dr. D. J. Jones

School of Chemistry, Bio21 Institute, University of Melbourne, Parkville, Victoria 3010, Australia

E-mail: djjones@unimelb.edu.au

Dr. L. Goerigk, Prof. K. P. Ghiggino, Prof. T. A. Smith
School of Chemistry, University of Melbourne, Parkville, Victoria 3010, Australia.

Dr. M. Liu, A/Prof. Y. Tachibana
School of Engineering, RMIT University, Bundoora, Victoria 3083, Australia.

Keywords: singlet fission, photophysics, organic photovoltaics, self-assembly core, liquid crystalline

Solution and solution-deposited thin films of the discotic liquid crystalline electron acceptor-donor-acceptor (A-D-A) p-type organic semiconductor FHBC(TDPP)$_2$, synthesized by coupling thienyl substituted diketopyrrolopyrrole (TDPP) onto a fluorenyl substituted hexa-*peri*-hexabenzocoronene

This is the author manuscript accepted for publication and has undergone full peer review but has not been through the copyediting, typesetting, pagination and proofreading process, which may lead to differences between this version and the Version of Record. Please cite this article as doi: 10.1002/aenm.201901069.

This article is protected by copyright. All rights reserved.

Author Manuscript

(FHBC) core, are examined by ultrafast and ns transient absorption spectroscopy, and time-resolved photoluminescence studies to examine their ability to support singlet fission (SF). GIWAX studies indicate that as-cast thin films of FHBC$(TDPP)_2$ are "amorphous", while hexagonal packed discotic liquid crystalline films evolve during thermal annealing. SF in as-cast thin films is observed with a ~150% triplet generation yield. Thermally annealing the thin films improves SF yields up to 170%. The as-cast thin films show no long-range order, indicating a new class of SF material where the requirement for local order and strong near neighbor coupling has been removed. Generation of long-lived triplets (μs) suggest these materials may also be suitable for inclusion in organic solar cells to enhance performance.

Author Manuscript

1. Introduction

The dominant loss mechanism in single-junction photovoltaic (PV) devices following excitation with high energy photons is the wasted excess energy above the bandgap that is emitted as heat (thermalization losses), leading to a maximum theoretical efficiency of 32% for a single-junction PV; the Shockley-Queisser limit.[1,2] A process that has the potential to increase this limit to 45% is to use high energy photons to produce two electron-hole pairs following the absorption of a single photon . In organic materials, such a photophysical process is called singlet fission (SF), the spin allowed conversion of a singlet excited state into two triplets by an assembly of two or more chromophores.[3] Although the mechanism of SF is not yet fully understood and is still the subject of intense research, it is generally accepted that the single excitation converts to a triplet pair state (^{1}TT), either coherently or incoherently, which later separates into two independent triplets ($2\times T_1$).[4,5] Recent studies show that the correlated triplet pair (^{1}TT) state may convert first to a spatially separated triplet pair intermediate ^{1}(T…T) before it undergoes dephasing or decorrelation into two independent triplets.[4]

The design of a chromophore capable of supporting SF requires optimization of both energetics and intermolecular electronic coupling, so there are only a limited number of reported SF systems.[6] For SF the energy of the singlet state ($E(S_1)$) should be greater than or equal to twice the energy of the triplet state ($E(T_1)$), i.e. $E(S_1) \geq 2E(T_1)$. Also, the electronic coupling between nearest neighbors must be optimized to have efficient SF. Singlet fission was first observed in crystalline anthracene, and has been extensively studied in this molecular system.[2] SF has since been reported with high yields in polyacenes,[7,8] such as tetracene, pentacene and their derivatives, oligophenyls,[9] diphenylisobenzofuran,[10] carotenoids,[11,12] rylene-based chromophores,[13] perylenediimides,[14] diketopyrrolopyrroles derivatives and some conjugated polymers.[15,16] Efficient SF has been reported mainly in condensed matter systems, e.g. crystals,[17-20] polycrystalline films,[21-23] amorphous films,[24,25] nanoparticles and aggregates.[12,26] Although SF has been reported in a limited number of partially disordered systems, highly efficient SF requires systems with a large degree of crystallinity and the SF yield is highly sensitive to the crystallinity of the film, crystal packing and intermolecular nearest-neighbor coupling in these systems; the so called "local-order constraint".[27] Theoretical calculations show that a slippage of only 2-3 Ångströms along the main acene axis can significantly reduce orbital overlap reducing SF yields.[28] It has been found that SF is suppressed in polymorphs with geometries that differ from their usual crystal packing arrangements.[25] For example, no SF in pentacene is reported for films grown on a polymer substrate, whereas the vapor deposited pentacene

This article is protected by copyright. All rights reserved.

films show efficient SF.[29,30] During attempts to improve photovoltaic devices by inclusion of SF materials (tetracene and pentacene) external quantum efficiencies of over 100% have been reported, however, these efforts resulted in only modest improvements in the device efficiency.[5] These results suggest the potential to enhance photovoltaic efficiency upon inclusion of SF materials, however, the sensitivity of device performance to the chromophore packing and the morphology of the active layer indicate new materials are required where the "local-order constraint" can be overcome. Recent studies using bridged acenes have demonstrated the key steric or conformational requirements for SF, and the need for spatially close chromophores that are electronically linked.[31-34] However, most of these studies were carried out in solution and often no mention was made of their SF yield in the solid state, which is important for practical exploitation. As a result, finding a system capable of efficient SF in films with a degree of molecular disorder can make the future production of commercial SF-based organic photovoltaic (OPVs) possible.

We aimed to develop a new class of solution processible SF materials that are more amenable to inclusion into solar cell devices through intra-molecular SF, and removal of the "local-order constraint". In this study, we investigate the use of hexa-peri-hexabenzocoronene (HBC) as a self-organizing core to promote singlet fission in amorphous films. HBC is a polycyclic aromatic hydrocarbon made up of thirteen fused six membered rings, which forms a mesophase. Soluble HBC derivatives show strong self-association in solution and discotic columnar structures with ordered morphology in films.[35] The HBC core shows strong π–π intermolecular association and can show high charge mobilities (ca. 1 $cm^2V^{-1}s^{-1}$ in certain silyl-substituted HBCs using pulse-radiolysis time resolved microwave conductivity measurements).[36] Substitution of HBC with 9,9-dioctylfluorene (FHBC) imparts solubility and the ability to form mixtures with other conjugated molecules. The diketopyrrolopyrrole (DPP) family consists of a class of dyes that have strong visible absorption, high stability, are synthetically tunable, highly fluorescent, and also have high exciton mobilities.[37] These properties make DPP derivatives good candidates for OPVs. Mauck et. al. observed SF for the first time in DPP derivatives with a yield of up to 200% in polycrystalline films.[37,38] Their studies on substituent variation in crystalline diketopyrrolopyrroles demonstrated that the torsion induced on substitution of thienyl (TDPP) by phenyl (PDPP) is sufficient to increase the π–π stacking distance and completely shut down SF, so SF in DPP is very sensitive to local-order (intermolecular coupling), which is not ideal for inclusion in OPV devices.[38] Our interest in developing solution processible SF materials for use for printed organic solar cells, led us to question, can we use the liquid crystallinity inherent in FHBC as a self-organizing motif and scaffold to pre-organize the DPP chromophore to promote intra-molecular SF in amorphous thin films? In this way can the "local-order constraint", inherent in known molecular SF materials, be removed?

Author Manuscript

This article is protected by copyright. All rights reserved.

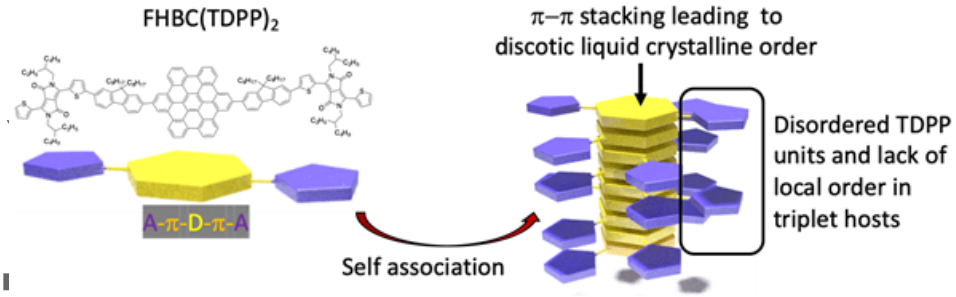

Figure 1. Chemical structure of FHBC(TDPP)$_2$ with a schematic representation of the A-π-D-π-A structure. The hexabenzocoronene (HBC, core D) provides strong self-association promoting discotic liquid crystalline order. The TDPP units, acting as triplet hosts, remain disordered removing any local order-based strong near-neighbor coupling for the dithienyldiketopyrrolopyrrole (TDPP, A) electron acceptor units.

The SF process has also been observed in a number of polymeric systems,[34,39,40] however, we wished to avoid polymeric SF materials to better understand the SF process as systematic structural modifications in polymers were expected to be significantly more challenging than in more defined smaller molecules. A significant potential advance in the field was suggested by Busby et al. in 2015 where they suggested that electron acceptor-donor-acceptor (A-D-A) type molecules may be a class of materials that could promote SF.[27] It was suggested that SF could be mediated in these systems through a charge transfer (CT) state , and by using intra-molecular systems it may be possible to overcome the "local-order constraint".[27] They demonstrated the development of SF materials, both molecular and polymeric, albeit with low singlet fission yields for the molecular systems in solution (56%). We have published a number of analogous A-D-A materials, our benzodithiophene-X-thiophene-rhodanine (BXR) series, as *p*-type organic semiconductors in organic solar cells,[41] however, calculations indicate that the triplet energy levels of these BXR materials are too high to support SF. Using this concept, we recently demonstrated that it was feasible to generate a new SF material by coupling two thienyl substituted diketopyrrolopyrroles (TDPP) to the benzodithiophene core (BDT), (BDT(TDPP)$_2$).[42] However, triplet generation was low in the solid state in the molecular donor at 18% efficiency, although results in solution suggested that the BDT(TDPP)$_2$ supported intra-molecular SF. The results indicated two key issues with BDT(TDPP)$_2$; i) the S_1 energy was possibly too low at 1.89 eV, barely 2 x T_1 (T_1 = 0.95 eV), and ii) no evidence for self-association was observed. These results suggested that a stronger driver is required for self-association and a higher S_1 energy along with the two TDPP triplet host acceptors were needed to increase the SF yield. In this study, the occurrence of SF in a hybrid material composed of FHBC as a self-organizing electron donor attached to TDPP as an electron acceptor was investigated.

We report here our studies on the discotic liquid crystalline material FHBC(TDPP)$_2$, comprising a fluorenyl substituted hexabenzocoronene (FHBC) core and two pendant bisthiophene-2,5-dihydropyrrolo[3,4-c]pyrrole-1,4-dione (TDPP) groups, for which we demonstrate a high SF yield in the solid state in as-cast and annealed films. We first reported FHBC(TDPP)$_2$ in 2012 as a *p*-type donor in organic solar cells.[43] FHBC(TDPP)$_2$ shows strong self-association in solution, and the hexabenzocoronene core provides a strong driving force to form hexagonally packed discotic liquid crystalline structures in melt extruded fibers. Thin film GIWAXS studies on FHBC(TDPP)$_2$ indicated

Author Manuscript

This article is protected by copyright. All rights reserved.

some π–π stacking, but little order other than this, suggesting strong self-association through the HBC units but little chance to order the pendant arms during spin coating, removing any local order between the TDPP units, **Figure 1**. The HOMO (highest occupied molecular orbitals) and LUMO (lowest unoccupied molecular orbitals) levels were reported at -5.40 eV and -3.40 eV respectively giving an energy gap of 2.00 eV. However, we did not report the triplet energy level of FHBC(TDPP)$_2$.

2. Results and Discussion

2.1. Film characterization

Grazing incidence wide-angle X-ray scattering (GIWAXS) measurements were performed on as-cast and thermally annealed thin films of FHBC(TDPP)$_2$ to gain information about the crystallization behavior in these films and structural changes upon thermal annealing. The resulting scattering patterns (**Figure 2**) indicate little or no crystalline order in as-cast thin films of FHBC(TDPP)$_2$ with no significant peaks in the GIWAXS (Figure 2A), that is, the films are effectively amorphous. The thermally annealed film of FHBC(TDPP)$_2$ shows the π-π scattering peak along the out of plane axis at 0.34 nm due to FHBC stacking (Figure 2B), while the scattering attributed to the lamella are oriented in plane with d-spacing of 2.9, 1.7 and 1.5 nm that is in agreement with our previous result of 2D GIWAXS measurements of melt extruded fibers.[43] The results suggest that FHBC(TDPP)$_2$ crystallites align in a face-on orientation. The crystallite dimensions for the thermally annealed film are summarized in Table S1 in the Supplementary Information.

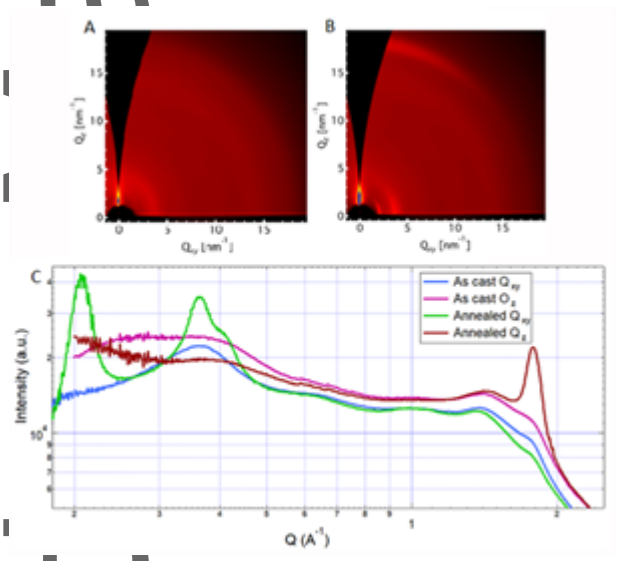

Figure 2. GIWAXS diffraction patterns of FHBC(TDPP)$_2$ A) as cast and B) thermally annealed films, and C) line cuts along the Q_{xy} and Q_z axes.

Author Manuscript

This article is protected by copyright. All rights reserved.

3.2. Triplet energy and structural character calculation

Time dependent density functional theory within the Tamm-Dancoff Approximation (TDA-DFT)[44] with the CAM-B3LYP functional[45] and natural-transition-orbitals (NTO) analyses were conducted to investigate the photophysical properties and excited state energy levels in FHBC(TDPP)$_2$. The structure of FHBC(TDPP)$_2$ is shown in Figure S1 and its xyz coordinates are reported in Table S2 in the Supplementary Information. The fluorene that is attached to the HBC core and thiophene ring is twisted at a dihedral angle of 40^o relative to the core. The results show that the first and second singlet excited states (S_1 and S_2) are quasi degenerate with vertical excitation energies of 2.84 and 2.86 eV and have oscillator strengths of 1.71 and 1.61, respectively. For these two singlet states, HOMO-1→ LUMO & LUMO+1 and HOMO→ LUMO & LUMO+1 excitations (**Figure 3**) are the respective dominant contributions with multiple minor contributions to the excitation energies stemming from other MOs. The HOMO is delocalized over the entire molecule, and the LUMO and LUMO+1 are localized on the DPP units and mostly located on the electron rich nitrogen and sulfur atoms. On the other hand, the HOMO-1 is located on the fluorene and DPP units. To find more information on the distribution patterns of electron and hole, the electron and hole NTO patterns for the S_1 state are demonstrated in Figure S2. The singlet state shows two main pair contributions where the electron and hole are mostly located on the fluorene and DPP units (Figure S2 A), and a minor component where the electron is delocalized over the whole molecule (Figure S2 B). These calculations suggest that the smaller atomic-orbital coefficients in the HBC core, and hence the lower contribution to the HOMO, might be due to the twist between the core and fluorene units. The NTO electron and hole pairs of the T_1 state are localized within the DPP unit (Figure S3). Moreover, the first triplet excited state (T_1) has a vertical excitation energy of 1.38 eV so FHBC(TDPP)$_2$ meets the energy level requirement for SF, i.e. $2*E(T_1) \leq E(S_1)$. Overall, however, the charge-transfer character of these excitations seems low. The same trends were confirmed with the ωB97X functional[46] (see Figure S4 in SI).

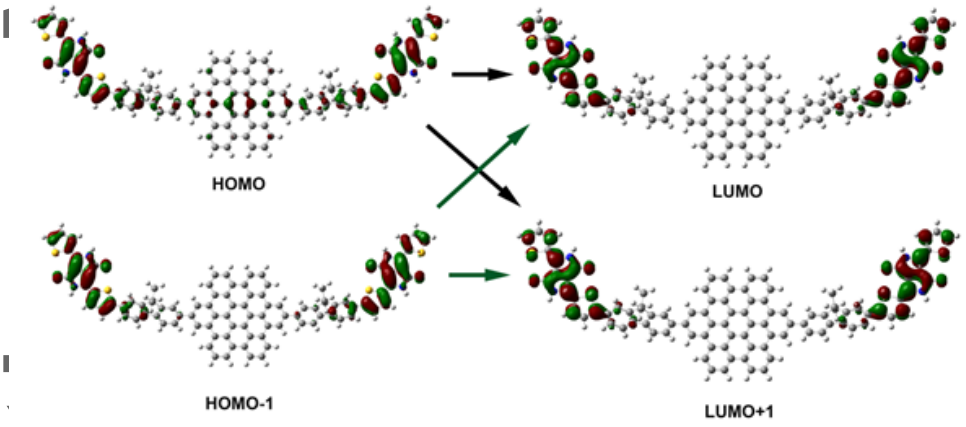

Figure 3. Representation of the main transitions in FHBC(TDPP)$_2$ where the HOMO is the highest occupied molecular orbital and LUMO is the lowest unoccupied molecular orbital.

2.3. Optical and electrochemical properties

Accepted Manuscript

This article is protected by copyright. All rights reserved.

Steady state absorption and fluorescence spectra of FHBC(TDPP)$_2$ were recorded for dilute chloroform solutions and in thin films (**Figure 4**). The absorption spectrum comprises a strong band at 365 nm, which can be assigned to the π-π^* transition of the FHBC component of the material, and a π-π^* intramolecular charge transfer absorption band at 580 nm. The absorption spectra of FHBC, TDPP and FHBC(TDPP)$_2$ in chloroform solution were also compared, see Supplementary Information Figure S5. The absorption spectrum of FHBC has a similar π-π^* transition band to FHBC(TDPP)$_2$ at 365 nm and the CT band in FHBC(TDPP)$_2$ shows a red shift of only 30 nm (550 to 580 nm) compared to free TDPP. FHBC(TDPP)$_2$ has a fluorescence quantum yield of about 30% in chloroform solution. In the photoluminescence emission spectrum, a sharp peak is seen at 627 nm in solution. We could not study the ionic character in the CT state in various solvents due to the solubility issue.

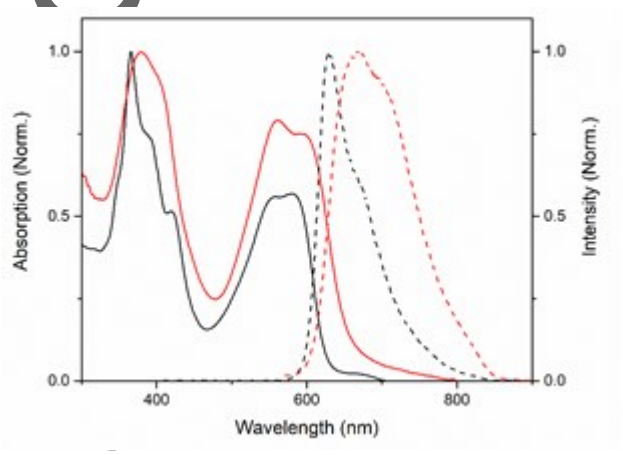

Figure 4. Normalized absorption (solid line) and fluorescence (dashed line) spectra of FHBC(TDPP)$_2$ in chloroform solution (black line) and thin film (red line).

In a thin film of FHBC(TDPP)$_2$ there is a slight broadening of the absorption bands, with a small redshift of the charge transfer band (≈20 nm) and the band at 365 nm becomes less featured. This suggests some aggregation in the thin film. It is known that FHBC(TDPP)$_2$ strongly associates in solution, and the small change in the FHBC π–π* transition on film formation suggests aggregates form that are not crystalline enough to show in the GIWAXS analysis. The steady state photoluminescence emission of the film is also broad and red-shifted compared to in solution, which suggests coupling between chromophores in the solid state. The broadened peak appears at 670 nm in thin film. The fluorescence quantum yield of the thin film is only about 1% indicating that there is an additional pathway for excited state quenching in the solid state that is not present in the solution. The absorption and fluorescence spectra of the thermally annealed film were recorded for comparison (see the Supplementary Information Figure S6 A and B). The bands narrow slightly in the annealed film with a 10 nm blue shift of the CT band compared to the as-cast film. This suggests that upon formation of a more ordered discotic liquid crystalline structure on annealing, as evidenced by the GIWAXS pattern (Figure 2B), there is no significant change in the FHBC environment, however, a less ordered TDPP environment is generated or there is less CT state coupling. On the other hand, the emission spectrum for the annealed film is quite similar to the as-cast film.

Author Manuscript

This article is protected by copyright. All rights reserved.

The optical bandgaps were calculated as 2.05 and 1.97 eV for FHBC(TDPP)$_2$ in the solution and thin film, respectively, from the intersection of the normalized absorption and emission spectra, see Figure 4.

The strong self-association, and optical bandgap of ≈2.0 eV[43] suggested this might be a good SF material, if the T_1 energy was in the range of 0.95-1.0 eV. Theoretical calculations show the S_1 and T_1 energy levels of 2.84 and 1.38 eV, respectively. The emission of FHBC(TDPP)$_2$ in thin film at room temperature and 77 K in the spectral region of 650-1400 nm and 900-1600 nm (with >1200 nm highpass filter) are shown in Figure S7. By decreasing the temperature to 77 K, the non-radiative loss pathways are frozen out,[47] and a peak appears at 1200-1400 nm (0.95 ev) which is assigned to the triplet state. It suggests that FHBC(TDPP)$_2$ has a T_1 energy level appropriate for SF.

It is expected that in a material that promotes SF, the photoinduced S_1 state will have a short lifetime as it undergoes SF to generate a correlated triplet pair. For the correlated T_1 states, the reverse triplet-triplet annihilation process will be fast unless the $E(S_1)$ energy is significantly above the energy of 2 x $E(T_1)$ state. Therefore, in an active SF material the T_1 state lifetime will be short when compared to a triplet generated through triplet sensitization experiments.

2.4. Time-resolved photoluminescence of FHBC(TDPP)$_2$ in solution and thin film

To provide more information about the decay kinetics of the singlet state the as-cast thin film and a dilute chloroform solution of FHBC(TDPP)$_2$ were characterized using time correlated single photon counting (TCSPC) measurements, see **Figure 5**. Following excitation at 400 nm, the fluorescence decays of FHBC(TDPP)$_2$ in the as-cast thin film and dilute chloroform solution show bi-exponential and single exponential decay behavior, respectively. The fluorescence of FHBC(TDPP)$_2$ in thin film decays very rapidly with $\tau_1 \approx$ 100 ps and $\tau_2 \approx$ 600 ps. On the other hand, the emission from FHBC(TDPP)$_2$ in dilute chloroform solution decays exponentially with a lifetime of ~2 ns, indicating that there is an excited deactivation pathway in the solid state that is not present in the solution.

Author Manuscript

This article is protected by copyright. All rights reserved.

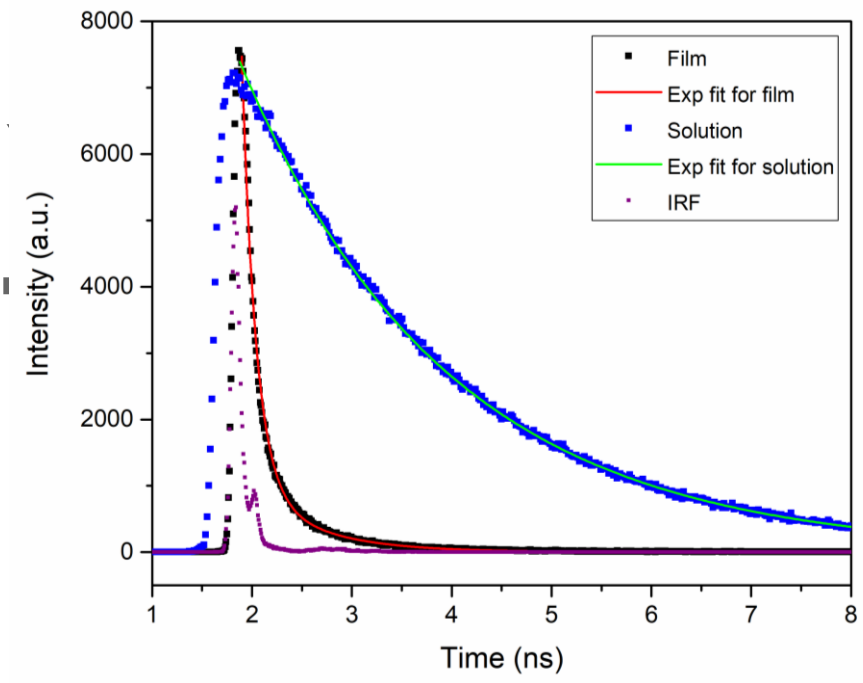

Figure 5. The instrument response function (IRF) and Fluorescence decay curves recorded by TCSPC, monitored at 650 nm following excitation at 400 nm for both thin film and dilute chloroform solution; the solid lines are the best fits using bi- and single exponential decay functions, respectively.

2.5. Femtosecond and nanosecond transient absorption in thin film and dilute solution

Femtosecond transient absorption (TA) measurements were undertaken to probe the excited state dynamics of FHBC(TDPP)$_2$ in dilute chloroform solution and thin film to better understand the contribution of uni- or bi-molecular interactions. The TA spectra and kinetic traces of FHBC(TDPP)$_2$ in both the visible (Vis) and near-infrared (NIR) regions following excitation at 600 nm in a dilute chloroform solution are shown in **Figure 6**A and B, respectively. A negative ground state bleach (GSB) signal was monitored in the region of 500-700 nm, mirroring the steady state absorption spectral features while positive transient absorption peaks at 760, 830, and 870 nm were recorded as PIA1, PIA2 and PIA3, respectively. The kinetics of PIA2 and 3 show biexponential decay kinetics with a rapid component and a slow component that decays over the nanosecond time window. The decay of PIA1 only shows the slow component. The transient signal of the GSB effectively mirrors the kinetics of PIA2 and 3 suggesting that a parallel two species process ($E_1 \rightarrow$ GS and $E_2 \rightarrow$ GS) is occurring in the solution of FHBC(TDPP)$_2$. To better understand the relationship between the PIA signals, we have completed a global target analysis (GTA) on the TA data to help identify the individual features and their population variation with time. The global analysis of the transient absorption data of FHBC(TDPP)$_2$ in the solution using a parallel two species process ($E_1 \rightarrow$ GS and $E_2 \rightarrow$ GS) returned the extracted spectra and kinetics of each species shown in Figures 6C and D, respectively. The extracted spectrum with a sharp peak at 850 nm (E_1 from GTA) decays with a time constant of ~30 ps. The extracted spectrum with an extra peak at around 760 nm (E_2 from GTA) decays over the nanosecond timescale. The results indicate that both E_1 and E_2 are generated upon excitation and relax

Author Manuscript

This article is protected by copyright. All rights reserved.

back to the ground state with different rates. We assign E_2 to the S_1 state as the results show the same kinetics for the ground state recovery (ns-TA) and the time-resolved fluorescence (TCSPC). E_1 is assigned to an excimer state, which is a short-lived component. The known π-π stacking of the FHBC core can lead to the formation of dimers even in a dilute solution of FHBC(TDPP)$_2$.

Nanosecond transient absorption (ns-TA) measurements were conducted to monitor the recovery of the ground state in FHBC(TDPP)$_2$ in solution. The kinetic trace at 650 nm following excitation at 600 nm, see Supplementary Information Figure S8, shows a single exponential decay with a time constant of about 3 ns, which matches the fluorescence decay profile from the TCSPC measurement. These results are consistent with the dominant mechanism in solution of FHBC(TDPP)$_2$ being a singlet state decay process back to the ground state with a competing parallel process, which also recovers the ground state with a much faster time constant. That is, no singlet fission is observed in solution.

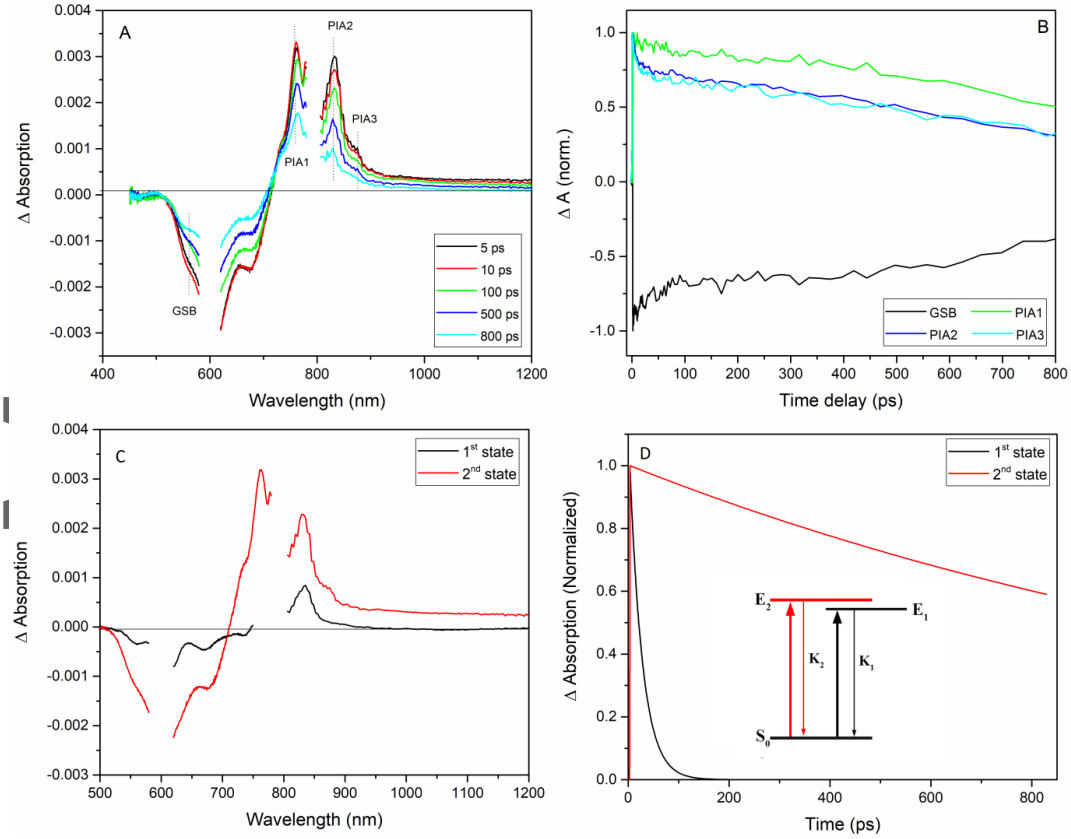

Figure 6. Transient absorption spectra at time delays of 5, 10, 100, 500 and 800 ps (A), and kinetic traces at 580, 760, 830 and 870 nm (B) of FHBC(TDPP)$_2$ in a chloroform solution after exciting at 600 nm with a fluence of 10 μJ/cm^2. (C) The associated spectra and (D) concentration profiles versus time for E_1 and E_2 from the global target analysis. The inset of graph C shows the extracted kinetic model.

This article is protected by copyright. All rights reserved.

To investigate the effect of the charge transfer state and chromophore association in solution, TCSPC measurements of solutions of FHBC(TDPP)$_2$ in various solvents and concentrations were performed. The fluorescence decay of FHBC(TDPP)$_2$ in solvents with various dielectric constants from toluene, chloroform, tetrahydrofuran and dichloromethane (ε = 2.4, 4.8, 7.5 and 9.1, respectively) are shown in the Supplementary Information Figure S9. Similar decay profiles were obtained for all of the solvents suggesting that no intrinsic pathway for rapid singlet state quenching in these solvents is observed, which is inconsistent with the expected fast depopulation of the S_1 state when SF is the dominant process. The fluorescence decay of FHBC(TDPP)$_2$ in chloroform solution with concentrations in the range 10-500 μM are shown in Figure S10. The results show no evidence for SF even at high concentration.

Femtosecond transient absorption (TA) measurements were performed on a thin film of FHBC(TDPP)$_2$ and the spectra extracted at time delays of 5, 10, 100, 500, 700, and 800 ps are shown in **Figure 7**A, along with decay traces for the GSB at 550 nm and positive photo-induced absorption at 760 (PIA1) and 900 nm (PIA2) (Figure 7B). The PIAs at 760 and 660 nm are expanded to 100 ps, inset Figure 7B, to highlight the difference in the initial transient behavior of these species. The GSB does not relax back to zero during the time-window of the experiment. The PIA2 has a rapid decay within the time region of 0-100 ps, while PIA1 has an initial fast decay similar to the PIA2 kinetics followed by a slower decay, Figure 7B. The kinetic trace of the GSB mirrors the kinetics of PIA1. Also, there is a growth of a positive transient signal at 660 nm following the initial decay of PIA1, inset Figure 7B. This evidence supports a sequential two-species process ($E_1 \rightarrow E_2 \rightarrow GS$) in the thin film of FHBC(TDPP)$_2$ so global target analysis was performed to help identify the individual features in the next section.

Author Manuscript

This article is protected by copyright. All rights reserved.

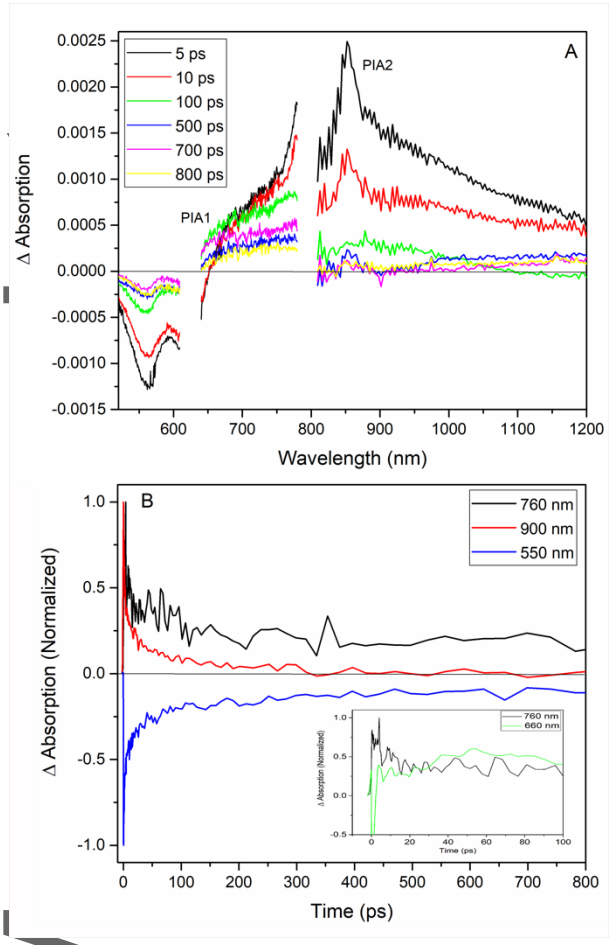

Figure 7. Transient absorption spectra at time delays of 5, 10, 100, 500, 700 and 800 ps (A), and kinetic traces at 550, 760 and 900 nm of FHBC(TDPP)2 in thin film after exciting at 620 nm (B) with a fluence of 10 μJ/cm2. The inset of Figure 7B shows PIAs at 760 and 660 ps expanded to 100 ps.

GTA was performed on the transient absorption data of $FHBC(TDPP)_2$ in the thin film using a simple, sequential two-species model ($E_1 \rightarrow E_2 \rightarrow GS$) as two independent species were recognized by a singular value decomposition (SVD) analysis. The extracted spectra and kinetics of the individual species are shown in **Figure 8**A and B, respectively. The broad extracted spectrum with a peak at 850 nm (E_1 from GTA, see inset Figure 8B) shows a rapid rise with a time constant of ~1 ps and decay with a time constant of ~10 ps. The extracted spectrum with a peak at around 760 nm (E_2 from GTA, see inset Figure 8B) has a delayed rise concomitant with the fall of the E_1 signal. Our GTA indicates a linear process with E_1 generated upon excitation, followed by population of the E_2 state with a slow relaxation to the ground state. We tentatively assign E_1 to the S_1 state and E_2 to the T_1 state following SF, however, to confirm this assignment we need to demonstrate that the E_2 spectrum corresponds to the $FHBC(TDPP)_2$ triplet state and the generated triplet pair lifetime is shorter than the isolated triplet.

Author Manuscript

This article is protected by copyright. All rights reserved.

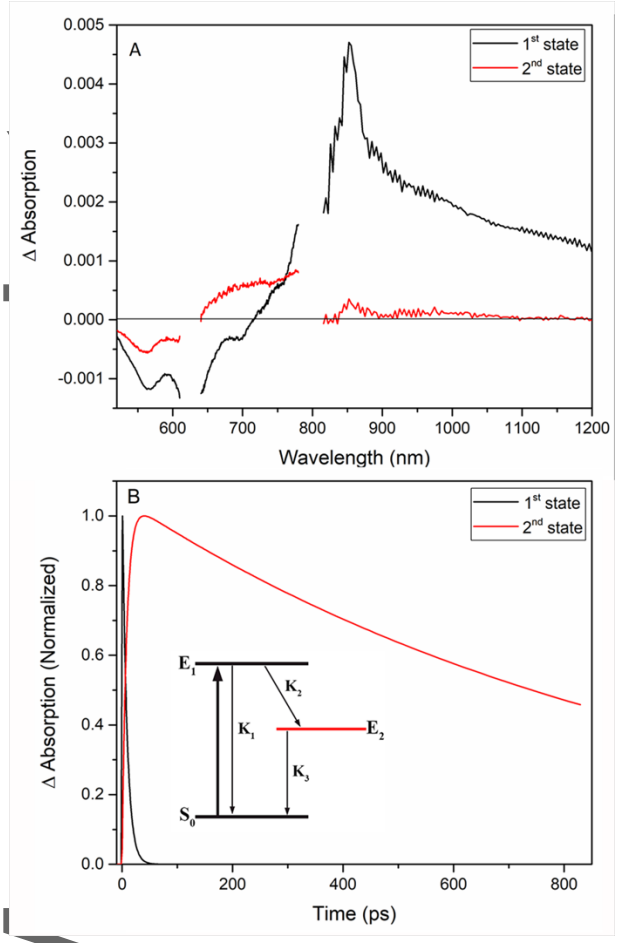

Figure 8. (A) The associated spectra and (B) concentration profiles versus time for E_1 and E_2 from the global target analysis for FHBC(TDPP)$_2$ in the thin film. The inset of Figure 8B shows the extracted kinetic model for FHBC(TDPP)$_2$ in thin film.

2.6. Triplet characterization

Triplet sensitization experiments have been undertaken to independently populate the triplet state and to find the excited triplet state absorption spectrum and isolated triplet lifetime in order to confirm that the long-lived species (E_2 from the GTA) formed after excitation of FHBC(TDPP)$_2$ is due to a triplet state. Palladium octaethylporphyrin (PdOEP) was chosen as the triplet sensitizer. Since PdOEP has two narrow and isolated absorption bands at 400 and 550 nm and they both overlap with the absorption band of FHBC(TDPP)$_2$, the sensitizer cannot be excited selectively. As a result, the sensitized transient absorption spectrum is a linear combination of the PdOEP, FHBC(TDPP)$_2$ triplet, and the non-sensitized FHBC(TDPP)$_2$ species. The TA spectra of PdOEP in a thin film show a narrow, negative ground state bleach (GSB) at 550 nm and no positive photoinduced absorption following excitation at 400 nm (Supplementary Information, Figure S11). As a result, the sensitized transient absorption spectrum is the combination of the non-sensitized spectrum and triplet energy transfer from the sensitizer to FHBC(TDPP)$_2$. To find the excited triplet state absorption, GTA was performed on the

Author

This article is protected by copyright. All rights reserved.

transient absorption data set of a FHBC(TDPP)$_2$:PdOEP blended film. The TA spectra of PdOEP sensitized FHBC(TDPP)$_2$ thin films (50:50 weight ratio) following excitation at 400 nm are shown in **Figure 9**A at different time delays. The kinetic traces of the sensitized and non-sensitized FHBC(TDPP)$_2$ films at selected wavelengths of 660 and 900 nm are shown in Figure 9B. The difference between the kinetic traces of PIA1 at 660 nm in the sensitized and non-sensitized FHBC(TDPP)$_2$ cases show that the triplet excited state of FHBC(TDPP)$_2$ gets repopulated over a time period of about 100 ps, and this is attributed to triplet energy transfer from the PdOEP to FHBC(TDPP)$_2$. The T_1-induced absorption spectrum extracted from GTA of the sensitization data (see Figure S12) is very similar to the long-lived species found in the pure FHBC(TDPP)$_2$ film (Figure 9C) suggesting that the long-lived species is a triplet rather than an excimer or any other long-lived, charge separated state. In conclusion, we confirm that triplets are formed on an ultrafast time scale following excitation of the FHBC(TDPP)$_2$ in the solid state.

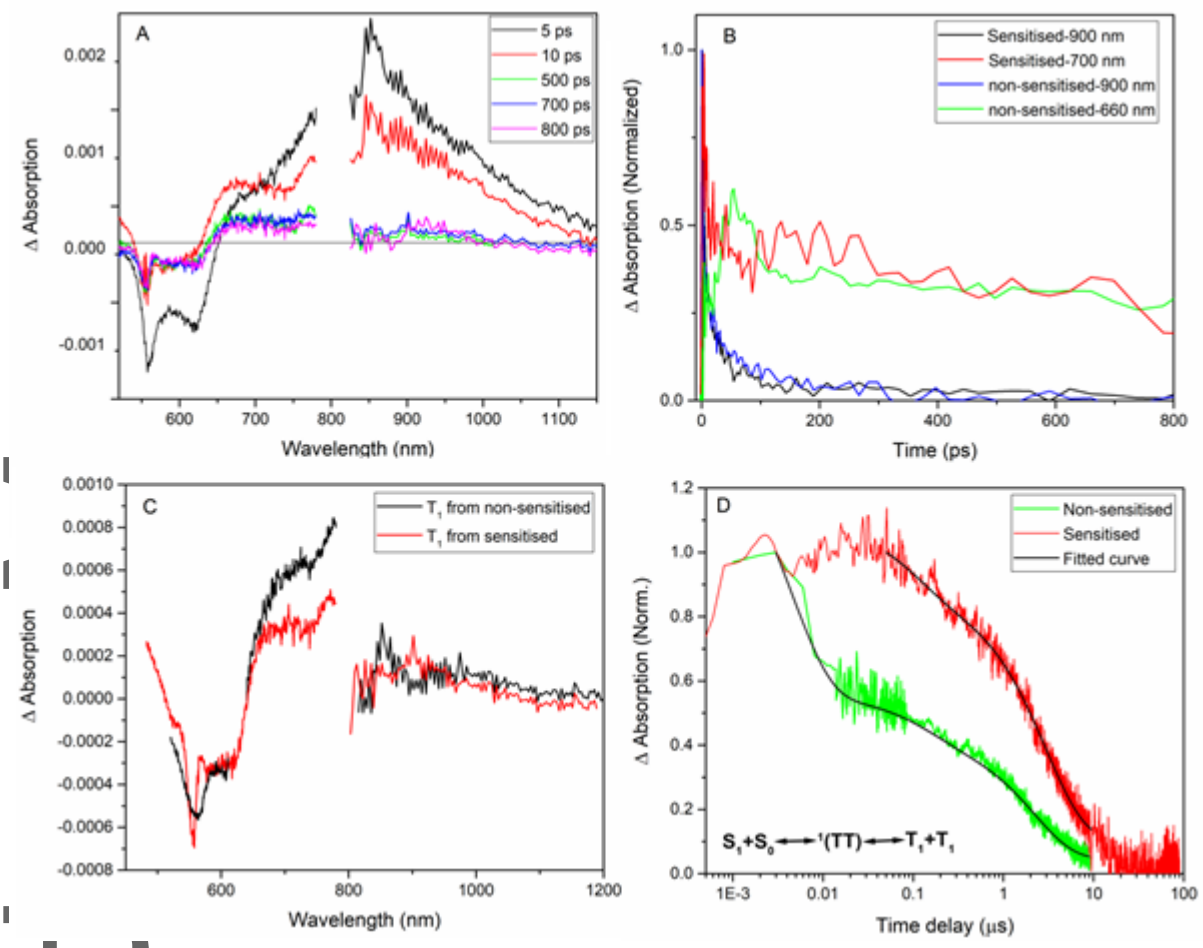

Figure 9. (A) Transient absorption spectra of sensitized FHBC(TDPP)$_2$ thin film at various time delays and (B) transient absorption decays at selected wavelengths (700 and 900 nm) of the sensitized and (660 and 900 nm) of non-sensitized thin films of FHBC(TDPP)$_2$, (C) T_1-induced absorption spectrum of the FHBC(TDPP)$_2$ derived from the triplet sensitization technique and associated spectrum of the 2nd excited state species from GTA. (D) Nanosecond transient absorption decays of sensitized and non-

This article is protected by copyright. All rights reserved.

sensitized thin films of FHBC(TDPP)$_2$ monitored at 730 nm following excitation at 550 nm with excitation density of 30 μJ/cm^2.

The fast triplet formation (<50 ps) in FHBC(TDPP)$_2$ as-cast films suggests SF rather than intersystem crossing (ISC) as the main mechanism of triplet formation, because in most cases ISC on such a short timescale is only observed in systems with heavy atoms.[27] To compare and provide more detail about the dynamics of the sensitizer-generated triplet species in FHBC(TDPP)$_2$ and triplets formed in the neat FHBC(TDPP)$_2$ film, nanosecond transient absorption (ns-TA) measurements were conducted on both FHBC(TDPP)$_2$ and FHBC(TDPP)$_2$:PdOEP blend films with excitation at 550 nm. The triplet absorption decays for both FHBC(TDPP)$_2$ and FHBC(TDPP)$_2$:PdOEP blend films were recorded at 730 nm (Figure 9D). The decay of the triplet transient signals for both films follow nonexponential kinetics. For FHBC(TDPP)$_2$, a three-component decay model, interpreted in terms of three separate states, provided the best fit to the data (Figure 9D). The lifetimes of the first and second triplet states were determined to be 5 ns and 140 ns, while the long-lived species has a lifetime of 2.5 μs. Two mechanisms have been proposed for triplet state formation through SF. First, the correlated triplet production can occur within two time scales, then it undergoes decorrelation to form individual triplets with 2 μs lifetime. The major population of the correlated triplet appears on the ps time scale after photoexcitation followed by a slower triplet growth over a few ns. According to the previous report of SF in a disordered film,[25] some of the chromophore dimer pairs have a favorable geometry that promotes SF. A singlet state around these sites can undergo SF whereas singlet excitons at other sites in the film can diffuse to those pairs forming a secondary diffusion-limited triplet production. The second mechanism, based on the suggestion made by Pensack et. al.,[4] is that the separation of the triplet pair requires the inclusion of an additional correlated intermediate. We assigned the first and second triplet states to two distinct correlated triplet pair intermediates as suggested by Pensack, whereas the third state is assigned to the decorrelated individual triplets.

The FHBC(TDPP)$_2$:PdOEP blend film also shows a biexponential decay with lifetimes of 100 ns and 3 μs. However, at the wavelength used, the FHBC(TDPP)$_2$ is excited directly as well as via the sensitizer, leading to two decay components. The triplet species with the longer time constants are attributed to the sensitizer generated individual triplets, which have similar lifetime to the slow decay component in the neat film. The rapidly decaying species are assigned to the correlated triplet formed by direct excitation of FHBC(TDPP)$_2$. A faster recombination rate for the triplet pairs generated from SF is due to the enhanced contribution of spin-allowed geminate triplet-triplet annihilation, which is confirmed by monitoring the delayed fluorescence compared to the sensitizer-generated single triplets, with a slower recombination rate. We recorded a long-lived emissive state at 620 and 750 nm that is assigned to delayed fluorescence as a result of geminate triplet-triplet annihilation, see Figure S13. The emission decays on the nanosecond time scale, well beyond the major excited singlet decay component of ~100 ps. The results are strongly suggestive that singlet fission occurs in the thin film of FHBC(TDPP)$_2$. The triplet yields for FHBC(TDPP)$_2$ in thin film were determined using the singlet depletion method, one of the well accepted methods of triplet yield determination. A triplet yield of 150% was calculated. This method has been used to calculate the triplet yield in various DPP derivatives, and has been shown to be comparable with triplet sensitization methods (more detail about the triplet yield calculation is provided in the Supplementary Information).

Author Manuscript

This article is protected by copyright. All rights reserved.

2.7. Femtosecond and nanosecond transient absorption in a thermally annealed thin film

To provide details about SF in the more crystalline film, TA measurements were performed on a thermally annealed thin film of FHBC(TDPP)$_2$. TA spectra at various time delays and extracted kinetic traces at 660 and 760 nm for the thermally annealed thin film of FHBC(TDPP)$_2$ are shown in **Figure 10**A and B, respectively. Global target analysis (GTA) was completed on the TA data of the thermally annealed thin film of FHBC(TDPP)$_2$ using a simple sequential two-species model ($S_1 \rightarrow T_1 \rightarrow GS$). The induced absorption peak at 700 nm, which is assigned to T_1 for the annealed thin film of FHBC(TDPP)$_2$, is slightly broader compared to the as-cast film. The results indicate that singlet fission occurs in the thermally annealed thin film of FHBC(TDPP)$_2$ with a triplet yield of 170% as measured by the singlet depletion method (details about the triplet yield calculation are provided in the Supplementary Information). Also, the thermally annealed thin film undergoes singlet fission with a faster rate constant of 0.2 ps^{-1} than the as-cast film with a rate constant of 0.1 ps^{-1}. The results suggest that increased stacking of FHBC units after annealing results in faster and more efficient SF.

Author Manuscript

This article is protected by copyright. All rights reserved.

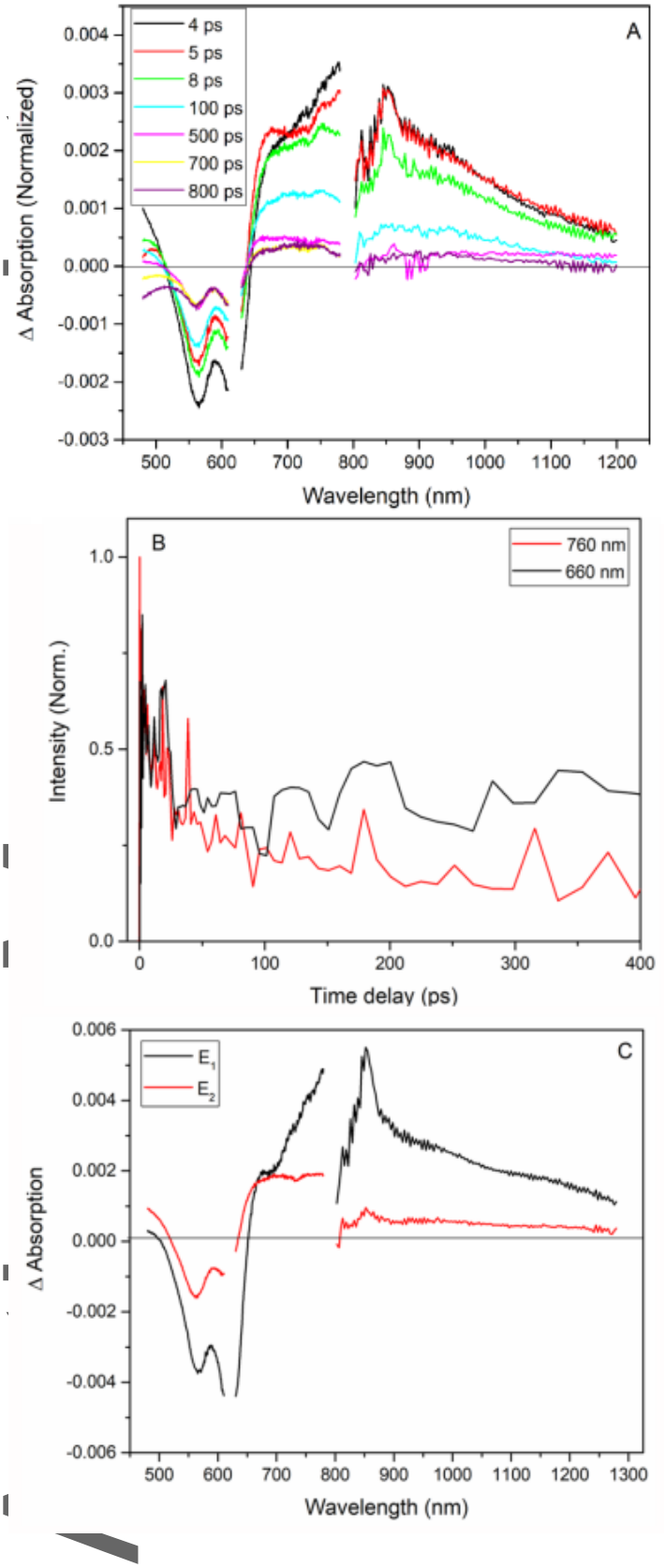

This article is protected by copyright. All rights reserved.

Figure 10. (A) Transient absorption spectra at various time delays and (B) transient decays at selected wavelengths of 660 and 760 nm of a thermally annealed FHBC(TDPP)$_2$ thin film, (C) The associated spectra for E_1 and E_2 from the global target analysis for the thermally annealed FHBC(TDPP)$_2$ thin film.

Author Manuscript

3. Conclusions

We have demonstrated the formation of SF-generated triplets in an "amorphous" as-cast FHBC(TDPP)$_2$ thin film, and evidence of de-coalescence of SF-generated triplet pairs is presented. We designed SF materials with an electron A-D-A structure to promote SF using liquid crystallinity as a self-organizing motif to pre-organize TDPP chromophores in amorphous films. It is suggested that the directed self-assembly through the HBC core and formation of discotic liquid crystalline domains, pre-organizes the TDPP chromophores (triplet hosts) in the solid state, placing them in close proximity but not allowing crystalline order; that is we have removed the "local-order constraint". The proximity allows Dexter energy transfer, and a potential route to the SF generated correlated triplet pair. Although GIWAX evidence suggests the as-cast films are amorphous, we have previously shown that FHBC(TDPP)$_2$ strongly associates in solution and therefore we suggest that aggregates form during drying, however, these aggregates are too small to strongly diffract. The rate of SF (0.1 to 0.2 ps^{-1}), the SF yield (150% to 170%), and molecular order are all improved upon annealing the film. We observe no evidence of SF in solution.

We believe that the use of liquid crystallinity as the self-assembly motif to drive self-organization for SF chromophores is a new pathway to new materials capable of singlet fission. Based on this idea, FHBC(TDPP)$_2$, comprising a hexabenzocoronene-fluorene (FHBC) core and two pendant bisthiophene-2,5-dihydropyrrolo[3,4-c]pyrrole-1,4-dione (TDPP) groups, with a low triplet energy level, was investigated for singlet fission. TDA-DFT calculations show that the first triplet excited state has an energy of about half of the first singlet excited state. The steady state photophysical measurements also confirm that this compound meets the energy level requirements for singlet fission. TCSPC, fs and ns transient absorption spectroscopy measurements were used to investigate the excited state dynamics in FHBC(TDPP)$_2$ in solution and film. Fast formation of the triplet state,

This article is protected by copyright. All rights reserved.

short lifetimes of the triplet pairs and delayed fluorescence in FHBC(TDPP)$_2$ in thin film suggest singlet fission is operating. The triplet pair lifetimes and the triplet yields are approximately 500 ns and 150%. GiWAXS measurements show well developed $\pi-\pi$ stacking peaks due to FHBC stacking but there is no apparent order in the TDPP moieties indicating a new class of SF material. This suggests that enhanced triplet harvesting may be possible in solar cell devices containing these materials and these device studies are currently in progress. We expect the results of this work can lead to the development of a new class of SF materials suitable for application in third generation optoelectronic devices and we are currently completing structure property studies to better understand the generation of triplets in these systems.

4. Experimental

4.1. Material synthesis

The commercially available chemicals were purchased from Sigma-Aldrich, Boron Molecular, Matrix Scientific, Ajax Finechem, Univar, Luminescence Technology Corp. and Suna Tech Inc. and all chemicals were used as received. FHBC(TDPP)$_2$ were prepared according to published procedures.[43]

4.2. Film Preparation

Glass substrates with dimensions of 2.5 cm × 2.5 cm × 0.1 cm were cleaned by sonicating sequentially in acetone, isopropanol and chloroform. Before thin film casting, the substrates were dried with a strong flow of nitrogen and then subjected to UV/ozone treatment for 30 min. Solutions of FHBC(TDPP)$_2$ were prepared by dissolving the samples into chloroform with a concentration of 5 mg/ml. To prepare blend films for sensitized experiments, solutions of FHBC(TDPP)$_2$ in chloroform mixed with palladium octaethyl porphyrin (PdOEP), were prepared by dissolving the compounds with mass ratio of 50:50. Finally, thin films were cast onto clean glass substrates via spin coating at 1000 rpm/s and spun for 1 min. The thermally annealed film was prepared by putting the as cast film on the top of a plate with the temperature of 120^o C for 10 min then the film was allowed to cool down to room temperature slowly.

Author Manuscript

This article is protected by copyright. All rights reserved.

4.3. Thin film characterization

Samples for grazing incidence wide angle X-ray scattering transmission measurements were prepared by loading the materials onto silicon wafers. The samples were analyzed at the SAXS/WAXS beamline at the Australian synchrotron[48] with an X-ray energy of 10 keV. A Pilatus 200K detector was used for wide-angle measurements. The substrates were silicon wafers that had been sonicated in acetone and isopropanol for 30 min each followed by 30 min of UV/ozone treatment. The beamline has a range of incident angles from Ω= 0.02−0.35 in 0.005 increments to allow signal optimization near the critical angle of the film but below the critical angle of the substrate. Data from GIWAXS experiments were analyzed using a customized version of NIKA 2D based in IgorPro.[49,50]

4.4. Steady state spectroscopy

Absorption spectra were recorded for FHBC$(TDPP)_2$ using a Varian Cary 50 UV−vis spectrophotometer. Fluorescence spectra were recorded on a Varian Eclipse spectrofluorimeter using an excitation wavelength of 550 nm and excitation and emission bandwidths of 5 nm for solution and 10 nm for film measurements.

Photoluminescence (PL) spectra in the near-IR region were recorded with a spectrometer (Horiba Jobin Yvon iHR320) and an amplified InGaAs photo-detector (Electro-Optical System). The excitation source was a supercontinuum laser (NKT Photonics, SuperK Extreme) for wavelengths tunable across the 450-750 nm region. The excitation beam was mechanically chopped and the detector output was fed into a lock-in amplifier synchronized to the chopper frequency. A 1200 nm high pass filter was used to remove the second order of the excitation and fluorescence. PL experiments at cryogenic temperatures were carried out in a liquid nitrogen cryostat (Oxford Instruments, Optistat DN).

4.5. Time correlated single photon counting

As described previously,[51] the excitation source was a mode-locked and cavity dumped Ti:Sapphire laser (Coherent Mira 900F/APE PulseSwitch) pumped by a Coherent Verdi-10 DPSS Nd:YVO_4 laser. The laser output (880 nm wavelength, 5.4 MHz repetition rate) was frequency doubled to provide an excitation wavelength of 440 nm. The individual fluorescence decay curves were collected using a time-correlated single photon counting (TCSPC) module (SPC-150, Becker & Hickl, Berlin, Germany). The fluorescence decay parameters were extracted from the decay profiles using FAST software (Edinburgh Instruments Ltd) and a sum of exponentials analysis.

4.6. Sub-nanosecond transient absorption spectroscopy

A mode-locked Ti:sapphire oscillator (Coherent, Mira Seed) seeded a Ti:sapphire regenerative amplifier system (Coherent, RegA 9050) to produce pulses of about 50 fs duration at a repetition rate

Author Manuscript

This article is protected by copyright. All rights reserved.

of 92 kHz and a wavelength centered at 800 nm. A portion of the light was used to generate the 400 nm pump beam using a β-BBO (β-barium borate) crystal, and the 630 and 730 nm pump beams were generated with an optical parametric amplifier (OPA9450, Coherent). The pump beam was mechanically chopped at ~3.5 kHz, and the arrival time of the pump pulses relative to the probe was manipulated using a variable optical delay line (Newport, UTS150PP with ESP 300 controller). The broadband probe was derived from the residual 800 nm beam focused onto a 3 mm sapphire substrate (Crystal Systems) for measurements in the visible region (450−800 nm) and a 5 mm undoped YAG substrate (Crystal Systems) for the infrared region (800−1400 nm). After passing through the sample, the probe beam was detected with a CMOS-equiped spectrometer (Ultrafast Systems) at 7077 spectra/s, and the excess 800 nm laser fundamental was blocked using low- and high-pass filters for the visible and IR regions, respectively. The relative orientation of the pump and probe polarization was 54.7° and all spectra were corrected for the chirp of the supercontinuum probe. Dry nitrogen was blown over films for all measurements.[52]

4.7. Nanosecond visible transient absorption measurements

Nanosecond visible transient absorption spectroscopy (ns-TA) was employed to monitor the triplet excited state lifetime. The measurements were conducted by a home-built transient absorption spectrometer with a N_2 laser (LTB Lasertechnik Berlin GmbH, MNL 202-C) pumped dye laser (LTB Lasertechnik Berlin GmbH, ATM200, 700 ps pulse duration) as an excitation source. Transient absorption was probed by a Xe lamp (Photon Technology International) light through two monochromators (Acton, Princeton Instruments), and detected by a Si based nanosecond detection system (Unisoku Co., Ltd., TSP-2000SN, time resolution: 1.2 ns (FWHM), monitoring wavelengths: 400-1,100 nm) with a fast oscilloscope (Tektronix, TDS 3052C, Digital Phosphor Oscilloscope 500 MHz 5 GS/s).[53] Transient data were collected with 550 nm excitation with a repetition rate of 2 Hz at 22 °C. The pulse excitation intensity was adjusted to 30 μJ/cm^2. Decay curve fitting was performed using FLASH software (Edinburgh Instruments Ltd) and an exponential components analysis.

4.8. Computational details

The geometry optimization of the ground state was carried out using Turbomole version 7.3[54] with the efficient hybrid-DFT model PBEh-3c[55] under inclusion of the continuum solvation model COSMO[56] to simulate the effects of chloroform as a solvent. In order to reduce computational costs, we have replaced the long side chains in the compound by methyl groups, as the length of the alkyl chains has no significant impact on the optical properties.[57] Vertical excitation energies were calculated via time dependent density functional theory within the Tamm-Dancoff Approximation (TDA-DFT)[44] using the CAM-B3LYP[45] range-separated hybrid functional approximation and the 6-311G**[58] atomic-orbital basis set based on the optimized geometry with the Gaussian09 program Rev. E.01.[59] A range-separated density functional approximation was chosen to ensure that potential charge-transfer (CT) states could also be appropriately treated. Moreover, it has been shown that this method is one of the most accurate hybrid functional approximations with an expected accuracy of 0.18 eV for medium-sized and large chromophores.[60] The pairs of hole and electron natural-transition-orbitals (NTOs)[61] for the S_1 and T_1 states were also calculated with Gaussian09 Rev. E.01.

Author Manuscript

This article is protected by copyright. All rights reserved.

Author Manuscript

Supporting Information

Supporting Information is available from the Wiley Online Library or from the author.

Acknowledgements

This work was made possible by support from the Australian Renewable Energy Agency which funds the project grants within the Australian Centre for Advanced Photovoltaics. Responsibility for the views, information or advice expressed herein is not accepted by the Australian Government. LG would also like to acknowledge generous allocations of computational resources from the University of Melbourne and the National Computational Infrastructure Facility within the National Computational Merit Allocation Scheme. We acknowledge the SAXS/WAXS beamline at the Australian Synchrotron. This work was partly supported by the JST PRESTO program (Photoenergy Conversion Systems and Materials for the Next Generation Solar Cells), Japan. We thank Dr Wallace W. H. Wong for the initial sample of FHBC$(TDPP)_2$ used in preliminary studies.

Received: ((will be filled in by the editorial staff))
Revised: ((will be filled in by the editorial staff))
Published online: ((will be filled in by the editorial staff))

References

[1] Rao and R. H. Friend, Nat. Rev. Mater., **2017**, *2*, 17063-17075.

This article is protected by copyright. All rights reserved.

[2] W. Shockley and H. J. Queisser, *J. Appl. Phys.*, **1961**, *32*, 510-519.

[3] M. B. Smith and J. Michl, *Chem. Rev.*, **2010**, *110*, 6891-6936.

[4] R. D. Pensack, E. E. Ostroumov, A. J. Tilley, S. Mazza, C. Grieco, K. J. Thorley, J. B. Asbury, D. S. Seferos, J. E. Anthony and G. D. Scholes, *J. Phys. Chem. Lett.*, **2016**, *7*, 2370-2375.

[5] J. Xia, S. N. Sanders, W. Cheng, J. Z. Low, J. Liu, L. M. Campos and T. Sun, *Adv. Mater.*, **2017**, *29*, 1601652-1601663.

[6] P. E. Hartnett, E. A. Margulies, C. M. Mauck, S. A. Miller, Y. Wu, Y.-L. Wu, T. J. Marks and M. R. Wasielewski, *J. Phys. Chem. B.*, **2016**, *120*, 1357-1366.

[7] J. J. Burdett and C. J. Bardeen, *J. Am. Chem. Soc.*, **2012**, *134*, 8597-8607.

[8] N. Geacintov, M. Pope and F. Vogel, *Phys. Rev. Lett.*, **1969**, *22*, 593-596.

[9] Zenz, G. Cerullo, G. Lanzani, W. Graupner, F. Meghdadi, G. Leising and S. De Silvestri, *Phys. Rev. B: Condens. Matter.*, **1999**, *59*, 14336-14341.

[10] Akdag, A. Wahab, P. Beran, L. Rulisek, P. I. Dron, J. Ludvik and J. Michl, *J. Org. Chem.*, **2015**, *80*, 80-89.

[11] C. Gradinaru, J. T. M. Kennis, E. Papagiannakis, I. H. M. van Stokkum, R. J. Cogdell, G. R. Fleming, R. A. Niederman and R. van Grondelle, *Proc. Natl. Acad. Sci.*, **2001**, *98*, 2364-2369.

[12] Wang and M. J. Tauber, *J. Am. Chem. Soc.*, **2010**, *132*, 13988-13991.

Author Manuscript

This article is protected by copyright. All rights reserved.

[13] E. Miller, M. R. Wasielewski and G. C. Schatz, *J. Phys. Chem. C.*, **2017**, *121*, 10345-10350.

[14] K. Le, J. A. Bender and S. T. Roberts, *J. Phys. Chem. Lett.*, **2016**, *7*, 4922-4928.

[15] U. Huynh, T. Basel, T. Xu, L. Lu, T. Zheng, L. Yu and V. Vardeny, in *SPIE NanoScience + Engineering*, SPIE, **2014**, 7.

[16] P. Tavan and K. Schulten, *Phys. Rev. B*, **1987**, *36*, 4337-4358.

[17] R. J. Dillon, G. B. Piland and C. J. Bardeen, *J. Am. Chem. Soc.*, **2013**, *135*, 17278-17281.

[18] R. E. Merrifield, P. Avakian and R. P. Groff, *Chem. Phys. Lett.*, **1969**, *3*, 155-157.

[19] G. B. Piland and C. J. Bardeen, *J. Phys. Chem. Lett.*, **2015**, *6*, 1841-1846.

[20] E. Swenberg and W. T. Stacy, *Chem. Phys. Lett.*, **1968**, *2*, 327-328.

[21] H. Arias, J. L. Ryerson, J. D. Cook, N. H. Damrauer and J. C. Johnson, *Chem. Sci.*, **2016**, *7*, 1185-1191.

[22] M. Grumstrup, J. C. Johnson and N. H. Damrauer, *Phys. Rev. Lett.*, **2010**, *105*, 257403-1-4.

[23] J. N. Schrauben, J. L. Ryerson, J. Michl and J. C. Johnson, *J. Am. Chem. Soc.*, **2014**, *136*, 7363-7373.

[24] G. B. Piland, J. J. Burdett, D. Kurunthu and C. J. Bardeen, *J. Phys. Chem. C*, **2013**, *117*, 1224-1236.

Author Manuscript

This article is protected by copyright. All rights reserved.

[25] S. T. Roberts, R. E. McAnally, J. N. Mastron, D. H. Webber, M. T. Whited, R. L. Brutchey, M. E. Thompson and S. E. Bradforth, *J. Am. Chem. Soc.*, **2012**, *134*, 6388-6400.

[26] J. N. Mastron, S. T. Roberts, R. E. McAnally, M. E. Thompson and S. E. Bradforth, *J. Phys. Chem. B*, **2013**, *117*, 15519-15526.

[27] Busby, J. Xia, Q. Wu, J. Z. Low, R. Song, J. R. Miller, X. Zhu, L. M. Campos and M. Y. Sfeir, *Nat. Mater.*, **2015**, *14*, 426-433.

[28] T. Nagami, S. Ito, T. Kubo and M. Nakano, *ACS Omega*, **2017**, *2*, 5095-5103.

[29] H. Marciniak, M. Fiebig, M. Huth, S. Schiefer, B. Nickel, F. Selmaier and S. Lochbrunner, *Phys. Rev. Lett.*, **2007**, *99*, 176402.

[30] H. Marciniak, I. Pugliesi, B. Nickel and S. Lochbrunner, *Phys. Rev. B*, **2009**, *79*, 235318.

[31] N. V. Korovina, S. Das, Z. Nett, X. Feng, J. Joy, R. Haiges, A. I. Krylov, S. E. Bradforth and M. E. Thompson, *J. Am. Chem. Soc.*, **2016**, *138*, 617-627.

[32] Kumarasamy, S. N. Sanders, M. J. Y. Tayebjee, A. Asadpoordarvish, T. J. H. Hele, E. G. Fuemmeler, A. B. Pun, L. M. Yablon, J. Z. Low, D. W. Paley, J. C. Dean, B. Choi, G. D. Scholes, M. L. Steigerwald, N. Ananth, D. R. McCamey, M. Y. Sfeir and L. M. Campos, *J. Am. Chem. Soc.*, **2017**, *139*, 12488-12494.

[33] S. Lukman, K. Chen, J. M. Hodgkiss, D. H. Turban, N. D. Hine, S. Dong, J. Wu, N. C. Greenham and A. J. Musser, *Nat. Commun.*, **2016**, *7*, 13622.

Author Manuscript

This article is protected by copyright. All rights reserved.

[34] S. N. Sanders, E. Kumarasamy, A. B. Pun, M. L. Steigerwald, M. Y. Sfeir and L. M. Campos, *Angew. Chem. Int. Ed.*, **2016**, *55*, 3373-3377.

[35] W. W. H. Wong, J. Subbiah, S. R. Puniredd, B. Purushothaman, W. Pisula, N. Kirby, K. Müllen, D. J. Jones and A. B. Holmes, *J. Mater. Chem.*, **2012**, *22*, 21131-21137.

[36] M. v. d. Craats, J. M. Warman, A. Fechtenkötter, J. D. Brand, M. A. Harbison and K. Müllen, *Adv. Mater.*, **1999**, *11*, 1469-1472.

[37] P. E. Hartnett, E. A. Margulies, C. M. Mauck, S. A. Miller, Y. Wu, Y.-L. Wu, T. J. Marks and M. R. Wasielewski, *J. Phys. Chem. B*, **2016**, *120*, 1357-1366.

[38] M. Mauck, P. E. Hartnett, E. A. Margulies, L. Ma, C. E. Miller, G. C. Schatz, T. J. Marks and M. R. Wasielewski, *J. Am. Chem. Soc.*, **2016**, *138*, 11749-11761.

[39] Y. Kasai, Y. Tamai, H. Ohkita, H. Benten and S. Ito, *J. Am. Chem. Soc.*, **2015**, *137*, 15980-15983.

[40] B. Pun, S. N. Sanders, E. Kumarasamy, M. Y. Sfeir, D. N. Congreve and L. M. Campos, *Adv. Mater.*, **2017**, *29*, 1701416.

[41] P. B. Geraghty, C. Lee, J. Subbiah, W. W. Wong, J. L. Banal, M. A. Jameel, T. A. Smith and D. J. Jones, *Beilstein J. Org. Chem.*, **2016**, *12*, 2298-2314.

[42] S. Masoomi-Godarzi, M. Liu, Y. Tachibana, L. Goerigk, K. P. Ghiggino, T. A. Smith and D. J. Jones, *Adv. Energy. Mater.*, **2018**, *8*, 1801720.

Author Manuscript

This article is protected by copyright. All rights reserved.

[43] W. W. H. Wong, J. Subbiah, S. R. Puniredd, B. Purushothaman, W. Pisula, N. Kirby, K. Muellen, D. J. Jones and A. B. Holmes, *J. Mater. Chem.*, **2012**, *22*, 21131-21137.

[44] S. Hirata and M. Head-Gordon, *Chem. Phys. Lett.*, **1999**, *314*, 291-299.

[45] T. Yanai, D. P. Tew and N. C. Handy, *Chem. Phys. Lett.*, **2004**, *393*, 51-57.

[46] J.-D. Chai and M. Head-Gordon, *J. Chem. Phys.*, **2008**, *128*, 084106.

[47] N. J. Turro, J. C. Scaiano and V. Ramamurthy, *Modern molecular photochemistry of organic molecules*, University Science Books, Sausalito, CA, **2010**.

[48] N. M. Kirby, S. T. Mudie, A. M. Hawley, D. J. Cookson, H. D. T. Mertens, N. Cowieson and V. Samardzic-Boban, *J. Appl. Crystallogr.*, **2013**, *4***6**, 1670-1680.

[49] Gann, X. Gao, C.-a. Di and C. R. McNeill, *Adv. Funct. Mater.*, **2014**, *24*, 7211-7220.

[50] J. Ilavsky, *J. Appl. Crystallogr.*, **2012**, *45*, 324-328.

[51] B. Zhang, H. Soleimaninejad, D. J. Jones, J. M. White, K. P. Ghiggino, T. A. Smith and W. W. H. Wong, *Chem. Mater.*, **2017**, *29*, 8395-8403.

[52] K. N. Schwarz, P. B. Geraghty, D. J. Jones, T. A. Smith and K. P. Ghiggino, *J. Phys. Chem. C.*, **2016**, *120*, 24002-24010.

[53] S. Makuta, M. Liu, M. Endo, H. Nishimura, A. Wakamiya and Y. Tachibana, *Chem. Comm.*, **2016**, *52*, 673-676.

[54] R. Ahlrichs, M. Bär, M. Häser, H. Horn and C. Kölmel, *Chem. Phys. Lett.*, **1989**, *162*, 165-169.

Author Manuscript

This article is protected by copyright. All rights reserved.

[55] S. Grimme, J. G. Brandenburg, C. Bannwarth and A. Hansen, *J. Chem. Phys.*, **2015**, *143*, 054107-1-19.

[56] Klamt and G. Schüürmann, *J. Chem. Soc., Perkin 2*, **1993**, 799-805.

[57] D. Chien, A. R. Molina, N. Abeyasinghe, O. P. Varnavski, T. Goodson and P. M. Zimmerman, *J. Phys. Chem. C.*, **2015**, *119*, 28258-28268.

[58] R. Krishnan, J. S. Binkley, R. Seeger and J. A. Pople, *J. Chem. Phys.*, **1980**, *72*, 650-654.

[59] M. J. Frisch, G. W. Trucks, H. B. Schlegel, G. E. Scuseria, M. A. Robb, J. R. Cheeseman, G. Scalmani, V. Barone, G. A. Petersson, H. Nakatsuji, X. Li, M. Caricato, A. V. Marenich, J. Bloino, B. G. Janesko, R. Gomperts, B. Mennucci, H. P. Hratchian, J. V. Ortiz, A. F. Izmaylov, J. L. Sonnenberg, Williams, F. Ding, F. Lipparini, F. Egidi, J. Goings, B. Peng, A. Petrone, T. Henderson, D. Ranasinghe, V. G. Zakrzewski, J. Gao, N. Rega, G. Zheng, W. Liang, M. Hada, M. Ehara, K. Toyota, R. Fukuda, J. Hasegawa, M. Ishida, T. Nakajima, Y. Honda, O. Kitao, H. Nakai, T. Vreven, K. Throssell, J. A. Montgomery Jr., J. E. Peralta, F. Ogliaro, M. J. Bearpark, J. J. Heyd, E. N. Brothers, K. N. Kudin, V. N. Staroverov, T. A. Keith, R. Kobayashi, J. Normand, K. Raghavachari, A. P. Rendell, J. C. Burant, S. S. Iyengar, J. Tomasi, M. Cossi, J. M. Millam, M. Klene, C. Adamo, R. Cammi, J. W. Ochterski, R. L. Martin, K. Morokuma, O. Farkas, J. B. Foresman, D. J. Fox, Gaussian 16 Rev. A.03 (Wallingford, CT, 2016).

[60] L. Goerigk and S. Grimme, *J. Chem. Phys.*, **2010**, *132*, 184103.

[61] R. L. Martin, *J. Chem. Phys.*, **2003**, *118*, 4775-4777.

Author Manuscript

This article is protected by copyright. All rights reserved.

Liquid crystallinity has been used in self-assembly of materials designed to support intra-molecular singlet fission (SF). Amorphous thin films of FHBC(TDPP)$_2$ show no long-range order, however 150% triplet yields are measured. Triplet yields are increased to 170% in hexagonally packed discotic liquid crystalline films formed after thermal annealing. The TDPP triplet hosts show no local order.

Keyword: singlet fission

Saghar Masoomi-Godarzi, Maning Liu, Yasuhiro Tachibana, Valerie D. Mitchell, Lars Goerigk, Kenneth P. Ghiggino, Trevor A. Smith and David J. Jones*

Liquid crystallinity as a self-assembly motif for high efficiency, solution processed, solid-state singlet fission materials

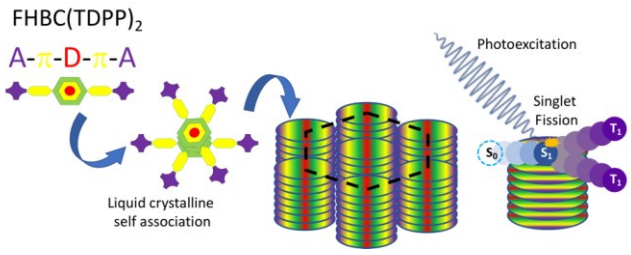

Author manuscript

This article is protected by copyright. All rights reserved.